Complex structural phase transition in a defect-populated two-dimensional system

A. V. Melechko,[1] M. V. Simkin,[1,*] N. F. Samatova,[2] J. Braun,[1,†] and E. W. Plummer[1]
[1]*Department of Physics and Astronomy, The University of Tennessee, Knoxville, Tennessee 37996 and Solid State Division, Oak Ridge National Laboratory, Oak Ridge, Tennessee 37831*
[2]*Computer Science and Mathematics Division, Oak Ridge National Laboratory, Oak Ridge, Tennessee 37831*
(Received 20 May 2001; published 29 November 2001)

A complex phase transition in Sn/Ge(111) and similar systems can be decomposed into two intertwined phase transitions: a structural symmetry lowering $(\sqrt{3}\times\sqrt{3})\Leftrightarrow(3\times3)$ transition and a disorder-order transition in the defect distribution. We present two phenomenological models that describe these transitions and their interrelation. These models allow us to understand the formation of domains and domain walls at low temperatures, defect-induced density waves above the structural transition temperature, and ordering of the defects caused by lattice-mediated defect-defect interactions. The models predict a destruction of the pure structural transition when impurities are introduced into the system, a shift in the structural crossover temperature with impurity density, and a dependence of the (3×3) lattice structure on the specific defect alignment.

DOI: 10.1103/PhysRevB.64.235424 PACS number(s): 68.35.Rh, 68.35.Bs, 71.45.Lr, 72.10.Fk

I. INTRODUCTION

The study of microscopic properties of phase transitions in low-dimensional systems provides an understanding of the fundamental aspects of systems of interacting particles. Phase transitions are strongly affected by defects, especially in systems with lower dimensionality. In quasi-one-dimensional (1D) or -2D systems that exhibit a charge-density wave (CDW) transition, a small proportion of microscopic disorder can control the global properties due to the collective nature of the phenomena.[1] Defects cause pretransitional effects, inducing the formation of the CDW. It has been speculated that the interaction of mobile defects with the CDW leads to alignment of defects with the CDW, or formation of defect density waves.[2] In this dynamic picture the distribution of defects is neither random nor static; instead defects align their positions to optimize the energy of the pinned CDW.[3]

The symmetry lowering phase transition $(\sqrt{3}\times\sqrt{3})\Leftrightarrow(3\times3)$ in Pb/Ge(111), Sn/Ge(111), and similar systems has been a subject of extensive studies.[5–29] These are quasi-two-dimensional systems composed of an ultrathin metal film on the surface of a semiconductor. At room temperature (RT), one-third of a monolayer of Sn is arranged in a $(\sqrt{3}\times\sqrt{3})R$ 30° structure on Ge(111) [referred to as a $(\sqrt{3}\times\sqrt{3})$ structure throughout this paper], with Sn atoms occupying the T_4 sites of the Ge(111) substrate,[30] as shown in Fig. 1. When the temperature is lowered, new (3×3) diffraction spots gradually appear in addition to the existing $(\sqrt{3}\times\sqrt{3})$ spots in a low-energy electron-diffraction (LEED) pattern.[7] Low-temperature (LT) scanning tunneling microscope (STM) images show (3×3) hexagonal (filled states) and honeycomb (empty states) complimentary patterns of bright atoms at biases of opposite sign. The (3×3) and $(\sqrt{3}\times\sqrt{3})$ unit cells are indicated in Fig. 1. The STM observations also display the presence of point defects in these surfaces, the majority of which are substitutional atoms (indicated in Fig. 1) from the substrate with vacancies constituting the rest.[19] In Sn/Ge(111), the density of the defects is in the range from 2% to 4% due to the preparation procedure, while in Sn/Si(111) and Pb/Ge(111) their density can be varied in a very wide range.[22,31]

In order to explain experimental observations, different models of the low- and high-temperature phases have been proposed. These models are based on the calculations of the ground state of these systems. First, based on the STM observations it was suggested that the low-temperature (3×3) phase in α phases of Pb/Ge(111) and Sn/Ge(111) was due to the stabilization of a surface CDW.[7,8] Later other models, such as the dynamical fluctuation model, were proposed.[5] First-principles calculations were invoked to support one or the other model. Even though the first-principles calculations are very insightful, they have been unable to describe the essential features of the local atomic scale structure observed by STM, due to the complexity and reduced symmetry created by the presence of defects. For example, plane-wave density-functional method calculations have predicted that for a defect-free system the (3×3) structure is the most stable by 5 meV per Sn atom.[5] It is reasonable to

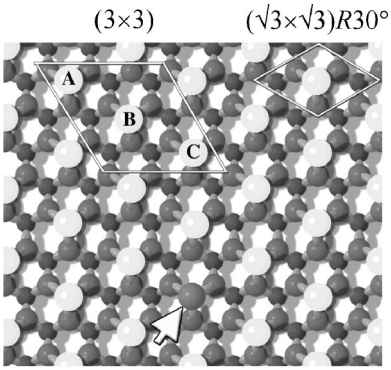

FIG. 1. Ball model of the $(\sqrt{3}\times\sqrt{3})$ Sn/Ge(111) structure. The light balls represent Sn atoms at the *T*4 sites of the Ge(111) substrate (dark balls represent the first double layer). The unit cells of the RT $(\sqrt{3}\times\sqrt{3})$ and LT (3×3) structures are shown in the right top and left top corners, respectively. The arrow at the bottom shows a substitutional point defect (Ge atom).

conclude that when the energy difference is so small any perturbation caused by the introduction of a defect can change the configuration of the ground state. Unfortunately, the real system with defects present is inhomogeneous and aperiodic. This makes it essentially untractable by first-principles methods due to high computational complexity. Therefore, phenomenological theories can fill an important gap between first-principles calculations and experimental observations. At this stage phenomenological models are essential for understanding the properties of the phase transition.

The two phenomenological models that are presented in this paper provide us with insight into the atomic evolution of these systems across the phase transition. The first model describes the disorder-order phase transition in the spatial defect distribution. It is based on the assumptions that (1) every defect induces local periodic lattice perturbation [called density wave (DW) hereafter], the decay length of which depends on the temperature and (2) DW-mediated defect-defect interactions force defects to move into positions to minimize the energy of the system.

The second model, referred to as the charge-compensation model (CCM), describes a structural $(\sqrt{3}\times\sqrt{3})\Leftrightarrow(3\times3)$ phase transition in a defect-populated system. By assuming, based upon experimental observation, that (1) the DW forms when temperature is lowered and that (2) the system responds to a charge impurity by inducing charge on its nearest neighbors, we can calculate the charge-density (CD) maps, which are compared directly to the STM images. The general approach developed in these models is not limited to a particular system or to a specific geometry (triangular 2D lattice in this work) and can be applied to other symmetry lowering displacive phase transitions in systems where defects are important. The models presented here are specifically applied to the case of the phase transition in the Sn/Ge(111) system, where comparison with STM data obtained earlier[19] will be used as justification for each model. The CD maps are interpreted as the STM images. Since STM images correspond to the 2D maps of the time-averaged local density of states (LDOS) that include both charge redistribution and accompanying lattice distortion, CD maps can be used to study the changes in the lattice structure as well.

It will be shown that defects control the structure and dynamics of these surfaces at all temperatures, inducing density waves at temperatures above the transition, pinning the waves, and controlling the domain structure below the transition temperature. Introduction of defects into the system destroys the pure structural phase transition. For the situation where the high- and low-temperature phases can still be distinguished such a gradual change is referred to as a crossover. It will be demonstrated that defects shift the crossover temperature. The nature of the accompanying defect-ordering controls the size of the domains at low temperature and the average arrangement of the atoms in the (3×3) unit cell (e.g., one up and two down or otherwise). The calculations based on the models presented here are consistent with the experimental results obtained from the spatial images of the surface (STM), and offer a clue to understanding the findings reported in the literature using momentum space probes such as x-ray and electron diffraction and angle-resolved photoemission.[4–6,11,25,26,29,32,33]

In the phenomenological treatment presented in this paper each atomic site is characterized by a parameter (called charge in the rest of the paper) that corresponds to an experimental observable such as the brightness of an atom in an STM image. The difference in brightness is due to a change in the LDOS that is a result of a time-averaged electronic redistribution, resulting from charge transfer, lattice distortions, or atomic fluctuations. Alternatively, this parameter could be presented in terms of time-averaged vertical displacement of each adatom. That is, we are not discussing the origin of the driving forces for the complex transition observed in these systems, but instead explain how defects control the nature of the transition. In contrast to previous reports we show here that the phase transition in Sn/Ge(111) is a complex phenomenon composed of two intertwined transitions: a second-order symmetry lowering structural $(\sqrt{3}\times\sqrt{3})\Leftrightarrow(3\times3)$ transition and a first-order defect-ordering transition. The structural phase transition is driven by short-range interactions intimately involved with the symmetry of the surface. The charge-compensation model is very similar to models used in description of magnetism (such as Ising). Compared to the Ising model, where it is assumed that the spin on a node can only have discrete values (e.g., $+1/2$ and $-1/2$), any value of charge is allowed in the CCM, bound only by the nature of the interaction and charge neutrality. So that, for example, we end up with configurations of charge on the three atoms in the unit cell in which two atoms have $1/2q$ and one $-q$, or one has $+q$, one 0, and one $-q$, or two have $-1/2q$ and one $+q$, but in all cases q can be any real number dictated by the equations of the model.

This paper is organized as follows. Section II describes the model of DW-mediated defect-ordering transition and results of Monte Carlo simulations. Section III presents a CCM and its interpretation in the framework of Ginzburg-Landau theory of phase transitions, as well as computer simulations of the STM images based on the CCM. Finally, our conclusions are presented in Sec. IV.

II. DEFECT-ORDERING TRANSITION: LINEAR SUPERPOSITION OF DEFECT-INDUCED WAVES AND INTERACTION OF DEFECTS

A. Observation of defect-ordering phase transition in Sn/Ge(111)

Before we proceed to the description of the defect-ordering transition model, the notation for different lattices must be introduced. The $(\sqrt{3}\times\sqrt{3})$ lattice can be completely covered by three (3×3) sublattices, because there are three Sn atoms in the (3×3) unit cell (Fig. 1). This is illustrated in Fig. 2. In this figure the brighter atoms indicate more negative charge and the darker atoms indicate more positive charge. The creation of a (3×3) sublattice from the original $(\sqrt{3}\times\sqrt{3})$ lattice with one bright and two dark atoms in the (3×3) unit cell is not unique, because three different (3×3) domains exist. It is easy to see how this happens from the structural model shown in Fig. 1. There are three Sn

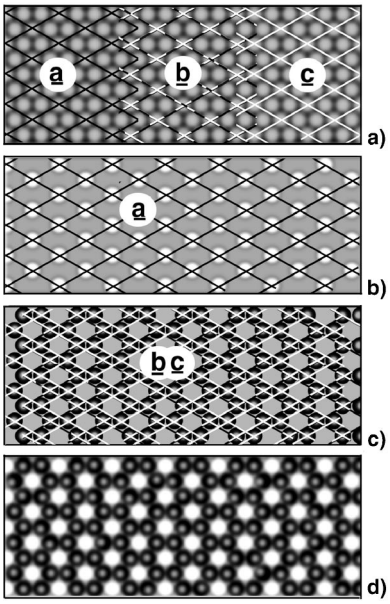

FIG. 2. Drawing of the three possible lattices associated with the (3×3) structure referenced to the original $(\sqrt{3}\times\sqrt{3})$ structure. (a) Three different options to lay (3×3) grids over a $(\sqrt{3}\times\sqrt{3})$ lattice that is represented by grey circles. Grids a, b, and c are illustrated by black, dashed, and white lines, respectively. (b) Hexagonal sublattice of corner atoms of the (3×3) structure coinciding with grid a in (a), called sublattice "A." (c) Honeycomb sublattice formed by the combination of sublattices b and c. (d) Combination of (b) and (c) results in a lattice that resembles the observed filled state low-temperature STM images.

atoms in the (3×3) unit cell, which have been labeled as A, B, and C. If atom A is negatively charged then B and C are positively charged, so that atom A forms a (3×3) hexagonal sublattice as seen in the STM filled state images. But it is equally probable that atom B (C) is negatively charged and atoms A and C (A and B) are positively charged, again forming a (3×3) hexagonal sublattice of B (C) atoms. Figure 2(a) illustrates the three different hexagonal sublattices [black grid (a), dashed grid (b), and white grid (c)], which cover the $(\sqrt{3}\times\sqrt{3})$ lattice (gray balls) completely.

It was experimentally determined that defects randomly distributed at RT become ordered at LT.[18] The STM measurements showed that inside one (3×3) domain at LT ($T\leqslant105$ K) defects are distributed on two sublattices out of three (e.g., only on B and C if the A's are charge-density maxima) while at temperatures $T\geqslant165$ K defects are distributed randomly on all three (3×3) sublattices. The correlation probability P_c is defined as the probability of observing on a small sampling area (randomly chosen) that all defects are aligned on two sublattices out of three. P_c was defined as 1 if all of the defects were aligned on two sublattices and 0 if they were random. P_c is an appropriate order parameter for the defect disorder-order transition (see Ref. 19 for details of the procedure).

B. Description of the model for defect-ordering phase transition

(1) Defects induce DW's in their vicinity. We make three basic assumptions with regard to the defect-induced waves that were inferred from experimental observations. The first is that the DW's induced by defects have a form of the exponentially decaying cosine functions.[19] The STM images[34] of Sn/Ge(111) at temperatures between 300 K and 105 K can be represented as a linear superposition of the decaying defect-induced waves.[18] These waves have the symmetry of the (3×3) state. Based on experimental observation, an ansatz for the DW's was proposed,

$$I(\mathbf{r})=f_{\sqrt{3}\times\sqrt{3}}(\mathbf{r})+\sum_{n}^{N_{def}}A_n e^{-|\mathrm{r}-\mathrm{r}_n|/l(T)}\sum_{i=1}^{3}\cos[\mathbf{k}_i(\mathbf{r}-\mathbf{r}_n)+\Phi_n]. \tag{1}$$

$I_{an}(\mathbf{r})$ is the brightness of an atom in the filled state image at a position $\mathbf{r}$; $f_{\sqrt{3}\times\sqrt{3}}$ models the $(\sqrt{3}\times\sqrt{3})$ periodicity of the STM images with no defects present. The second term on the right side of Eq. (1) consists of a sum over all attenuated waves induced by N_{def} defects with coordinates $\mathbf{r}_n$ and phases Φ_n. The phase Φ_n of the waves from a vacancy is chosen to be 0, and π for a Ge defect, based on experimental observations.[19] The amplitude A_n is constant for all defects. Figure 3(a) presents the direction of the (3×3) vectors $\mathbf{k}_i$ used in Eq. (1). Damping is taken into account by introducing the exponential factor with a decay length $l(T)$.

The second assumption is that the decay length of the defect-induced waves has a strong temperature dependence. The temperature dependence of the decay length $l(T)$ for Sn/Ge(111) was determined experimentally.[18] The behavior of its reciprocal value can be represented as

$$\frac{1}{l(T)}=\alpha\cdot T+\beta, \tag{2}$$

where $\alpha=3.85\times10^{-4}$ Å^{-1}K^{-1} and $\beta=-2.35\times10^{-2}$ Å^{-1}. The honeycomb pattern induced by one substitutional defect, simulated using Eq. (1), is shown in Fig. 3(b) for $l(T)=3d_{\sqrt{3}}$, where $d_{\sqrt{3}}$ is a lattice spacing between adatoms in the $(\sqrt{3}\times\sqrt{3})$ structure [$d_{\sqrt{3}}=7$ Å for Sn/Ge(111)]. If there is more than one defect in the surface then the defect-induced waves produce a very complex pattern as a result of a linear superposition of waves. For example, two defects [Fig. 3(c)] induce a honeycomb pattern in their immediate vicinity that gradually becomes hexagonal in the area between them [intersection of two circles that indicated decay length $l(T)=14d_{\sqrt{3}}$].

The third basic assumption about the properties of the defect-induced waves is that the absolute value of the charge modulation does not exceed a saturation limit. This assumption is made to overcome an unphysical artifact of using a simple linear superposition of waves from every defect in the ansatz, $I_{an}(\mathbf{r})$, [Eq. (1)] when the decay length is very large. In this case the amplitude could be proportional to the total number of defects. For example, if we had N_{def} defects on a surface aligned on one sublattice with the decay length close to infinity, the charge on one lattice site would be N_{def} times the intensity of the DW induced by one defect. This is not

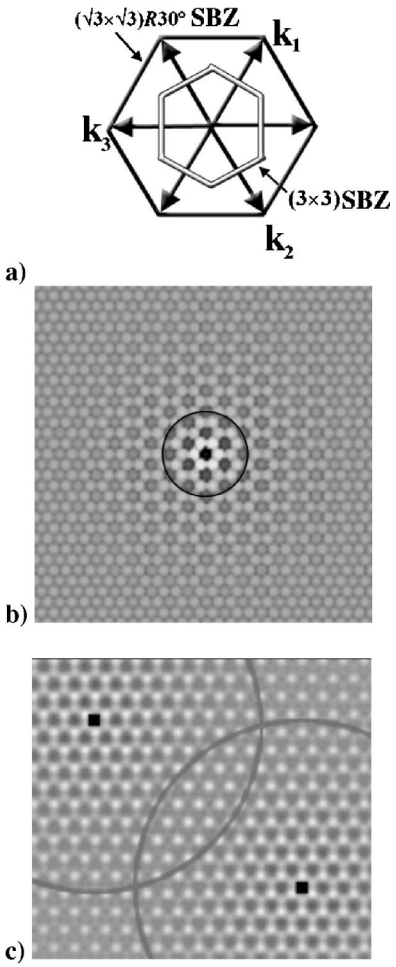

FIG. 3. Simulation of defect-induced waves using ansatz. (a) k vectors for the waves from the defects in Eq. (1). The surface Brillouin zones of both structures are shown. (b) Simulation of Ge defect-induced waves calculated using Eq. (1) for one defect $[l(T)=3d_{\sqrt{3}}, T_{Sn/Ge(111)}\approx 170\ \mathrm{K}]$. (c) Interference pattern of waves induced by two defects located on two different (3×3) sublattices $[l(T)=14d_{\sqrt{3}}, T_{Sn/Ge(111)}\approx 100\ \mathrm{K}]$.

physically reasonable and can be avoided by introducing saturation effects as follows. The amplitude $I_{an}(\mathbf{r})$ is recalculated as

$$I(\mathbf{r})=S(I_{an}(\mathbf{r})) \tag{3}$$

where $S(I)$ is some nonlinear monotonous function that doesn't let $I_{an}(\mathbf{r})$ exceed a saturation value I_{sat} on each site. We choose $S(I)$ to be a linear function that has a slope equal to 1 for small values of the argument and that approaches a constant I_{sat} when the argument is large.

(2) Defects interact with DW's induced by other defects. According to STM and surface core-level shifts data, Ge defects avoid more negatively charged lattice sites (bright sites in the filled state STM images). Ge defects energetically favor being positively charged. This observation sets the stage for an interaction between DW's (defect-induced or intrinsic) and defects, and is the basis of our model for a defect-ordering phase transition. If a defect is located on a negatively charged site, that is energetically unfavorable, there is a lateral force exerted on it toward a more positively charged site. This can be modeled by the assumption that the difference in energy for a defect to be on one site versus its nearest-neighboring site is proportional to the difference of the value of $I_{an}(\mathbf{r})$(i.e., charge density) on these sites:

$$\Delta E\approx I(\mathbf{r}_{def})-I(\mathbf{r}_{NN}). \tag{4}$$

If this difference exceeds an activation barrier E_a, the Ge defect exchanges its position with a neighboring Sn atom.

(3) There is a random thermal motion of defects. Since the experimental measurements showed that this is a reversible transition we must include a randomizing force of thermal motion of defects. This is accomplished by using Monte Carlo calculations.

Let us summarize all the premises of the model:

(i) Defects induce DW's that can be simulated using Eqs. (1) and (4).

(ii) Defects exchange positions with nearest-neighbor (NN) Sn atoms if the difference of energies [Eq. (3)] exceeds the activation barrier E_a. There is also a random thermal hopping included.

(iii) The range of the defect-defect interaction must have a strong temperature dependence, $l(T)$.

We investigated the parameter space of this model by performing Monte Carlo computer simulations. The following algorithm was used to perform the computations. Initially, N_{def} defects (defect density is a free parameter) are positioned randomly on the $(\sqrt{3}\times\sqrt{3})$ lattice. Then $I_{an}(\mathbf{r})$ is calculated using ansatz Eqs. (1) and (4). For each defect $I_{an}(\mathbf{r})$ is compared at the defect site with $I_{an}(\mathbf{r})$ at nearest-neighbor Sn sites and if this difference [Eq. (3)] is larger than a value of the activation barrier then this defect is moved to a new position. The minimum out of six NN's is chosen, and it is checked that this NN is not a defect. If the difference is smaller than a threshold value a Monte Carlo procedure is used to decide whether to move the defect or not, that is, a random number between 0 and 1 is generated, then this number is compared to the exponential factor $B_{MC}=a_f\exp(-E/kT)$, where $E=E_a-[I(\mathbf{r}_{def})-I(\mathbf{r}_{NN})]$, and $k=f_m k_B$ is a product of the Boltzman constant and a parameter f_m, which is a function of the mobility of defects. a_f is the attempt frequency. If this random number is smaller than the B_{MC} then this defect is moved to the nearest-neighbor position. The decay length is varied emulating a changing temperature, and the distribution of defects is measured by calculating the correlation probability P_c. The number of repeats at each temperature step controls the simulation of the cooling/warming speed. In the simulations this number was varied from 1 to 1000 for each temperature step (usually 1 K). More repeats are used to approach equilibrium at each temperature. To determine the cooling speed that corresponds to a particular simulation such parameters as the attempt frequency and the activation barrier must be assessed by experimental measurements or by a more fundamental calculation. This model requires the following input parameters: an attempt frequency (mobility of defects) f_m, density of defects ρ, activation barrier E_a, and temperature dependence of the decay length $l(T)$.

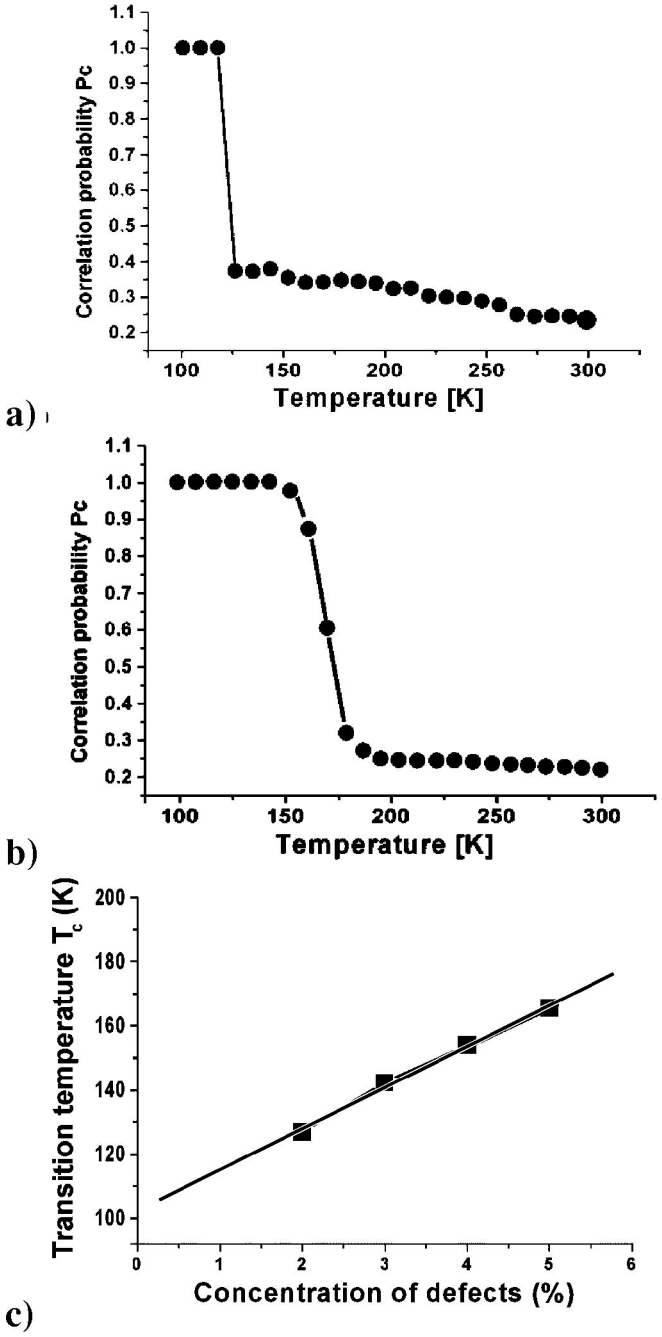

FIG. 4. Defect-ordering phase transition. (a) Temperature dependence of the order parameter P_c of the defect-ordering transition for a 2% defect density. (b) Temperature dependence of the order parameter P_c of the defect-ordering transition for a 5% defect density. (c) Dependence of the transition temperature on the density of defects.

C. Results of the simulations based on the defect-ordering transition model

(1) The model describes a first-order disorder-order phase transition. Figure 4(a) displays a result of a simulation for Sn/Ge(111) with $\rho=2\%$, $l(T)$ that was calculated using Eq. (2) with α and β determined from experiment, one repeat at each temperature step ($\Delta T=1$ K), and $E_a=0.95\times I_{sat}$. This simulation, with such a set of values of the free parameters, reproduces our experimental results: (1) a transition temperature for defect ordering $T_{DO}\approx 100$ K and (2) at low temperature the defects are completely ordered on two of the three sublattices. This calculation shows that this is a first-order phase transition since its order parameter appears discontinuously. Another signature of the first-order phase transitions, nucleation, can also be observed above the transition temperature in this model system. For small values of the decay length only defects that are in areas with slightly higher local defect density move into ordered positions. The local ordering is reflected in a nonzero slope of the curve in Fig. 4(a) at temperatures above T_{DO}. When the decay length reaches an average distance between defects something similar to the ''domino effect'' happens. Waves from defects that are already ordered are in phase. This leads to a strong influence on the defects that are not ordered, shifting them to the new positions so that the waves induced by these defects become in phase. Thus when the interaction length exceeds a critical value the ordering of defects propagates across the whole surface. This is the feature of a first-order phase transition.

(2) The transition temperature depends linearly on the defect density. Figure 4(b) contains a result of the calculation for 5% of defects with all other parameters kept the same as for 2% [Fig. 4(a)]. Clearly the transition occurs at a higher temperature. Figure 4(c) shows the dependence of the transition temperature on defect density, where the density of defects is varied in the range 2%–5%.

(3) Defects can order on one sublattice. It is interesting to note that for smaller values of the activation barrier E_a (relative to I_{sat}) defects order on one sublattice out of three, instead of two out of three. Also, if a much larger number of repeats (slower cooling) is used then the defects order on one (3×3) sublattice out of three, indicating that the ordering observed experimentally is a metastable (nonequilibrium) state of a defect distribution. Apparently, the ground state of the defect-ordered system is one where all of the defects within one domain are positioned on only one of the three possible lattices (Fig. 2).

III. STRUCTURAL PHASE TRANSITION IN A DEFECT-POPULATED SYSTEM

A. Charge-compensation model

The previous model for defect-induced waves describes all characteristics of the STM images of this system for temperatures above ≈ 100 K. The distinctive features that cannot be reproduced at lower temperatures are the very narrow boundaries between different (3×3) domains (Fig. 4 of Ref. 19). The phenomenological model introduced here allows us to calculate the charge redistribution as observed in STM images at all temperatures, including the temperatures where such sharp domain walls are observed. This model assumes a defect configuration and then calculates the charge distribution on all of the Sn atoms at any temperature, reproducing all STM observations.

The charge-compensation model is based on four assumptions. The first is that the charge on a lattice site is proportional to the sum of charges on its nearest neighbors. Let's

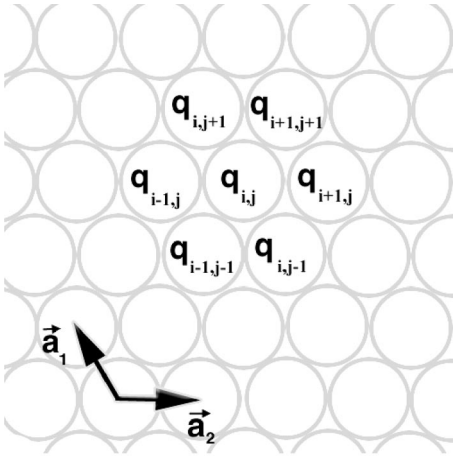

FIG. 5. The diagram of the charge-compensation model, where $q_{i,j}$ is the charge on the (i,j)th site. The lattice vectors of the unit cell are also shown as $\mathbf{a}_i$.

consider a two-dimensional triangular lattice as shown in Fig. 5. The unit vectors displayed in this figure define the $(\sqrt{3}\times\sqrt{3})$ periodicity (to be consistent with the experimental observations where the notations for superstructures are chosen with respect to bulk). Let's suppose that nearest-neighbor (NN) interaction is such that the charge on site (i,j), indicated in Fig. 5, is determined by the following equation:

$$q_{i,j} = -R(T)\cdot \sum_{k,l=NN's}^{6} q_{k,l}, \tag{5}$$

Here $R(T)$ is the charge-compensation factor (CCF), a free parameter that we assume is a monotonous function of temperature. The summation goes over the six nearest neighbors shown in Fig. 5. In other words, when a charge is placed on one of the atoms, its nearest neighbors will try to screen or ''compensate'' for its charge.

The second premise is that the absolute value of charge on any lattice site has a saturation value. Coulomb repulsion should make it increasingly more difficult to add charge to one atom. This can be accounted for by adding a saturation term to Eq. (5):

$$q_{i,j} = -R(T)\cdot \sum_{k,l=NN's}^{6} q_{k,l} - s(q_{i,j}), \tag{6}$$

where $s(q)$ must be an odd function. The first nonlinear term in the polynomial that can be used for this purpose is cubic:

$$s(q) = a_3 q^3. \tag{7}$$

Here a_3 is a parameter that is assumed to be small and positive $(0<a_3\ll 1)$.

The third assumption is that the charge on the lattice site corresponding to a defect (Ge substitutional atoms or vacancies) is fixed, the same for all defects of one type (positive for Ge defects and negative for vacancies), and independent of its position in the lattice, the temperature, and the defect density.

Finally, the fourth and last assumption is that the total charge of the system is always zero. The results presented in this paper are obtained with calculations where charge neutrality was required locally. This was accomplished by the following algorithm. When a new value for a charge on an atom is calculated in each iteration, the difference of charges between the new and the old value is drawn from the NN atoms. Even though in most of the calculations the condition of charge neutrality of the system was imposed, it is interesting to note that when charge neutrality was not imposed on the system, it still remained neutral in cases where the initial (before the iterations) total charge was zero, i.e., N defects and N Sn atoms with opposite charge. Moreover, even if the initial conditions were such that the total charge was not zero, i.e., N negatively charged defects only, after a few iterations (without imposing charge neutrality) the system relaxed to a neutral state with the total charge oscillating in the vicinity of zero.

To calculate a charge-density map for a given distribution of defects and certain values of $R(T)$ and a_3, the charge on every atom is calculated self-consistently using Eqs. (6) and (7). First, some initial distribution of charge (usually random with total charge equal to zero) is generated for all atoms. The charge on the first atom is calculated using Eqs. (6) and (7). Then the same calculation is performed for its next-nearest neighbor and so on for all atoms in a surface. This procedure is repeated until a self-consistent solution is reached. If the lattice site corresponds to a defect, the charge is set to a fixed value. Essentially, defects are treated as a part of the boundary conditions in this problem. The same procedure is repeated for all atoms many times. To reduce the influence of the boundaries, calculations were made for a large number of atoms with the area under consideration located in the middle of a larger area. The charges of atoms outside the calculated area were chosen to be zero. The application of periodic boundary conditions does not change the results of the calculation from the zero charge boundary conditions. The solution is less sensitive to the boundaries for a larger number of defects.[35] The results were obtained by computer simulations based on the CCM. The free parameters of this model are

(i) charge on a defect, q_{def}; we always used $q_{def}=+1$ for Ge defects and $q_{def}=-1$ for vacancies. The variation of this parameter doesn't change the results qualitatively;

(ii) charge-compensation factor, R;

(iii) saturation parameter a_3 ($a_3=0.1$ for all simulations presented here); and

(iv) number of defects N_{def} and their positions.

B. Results of the calculations based on the CCM

Simulations with the CCM indicate that the critical value of R is 1/3 (see the following). For $R<1/3$ the high-temperature STM images could be reproduced and the CCM could be mapped onto the previous DW model. For $R>1/3$ all of the features such as domains and sharp domain boundaries in the low-temperature STM images could be reproduced. The critical temperature T_{ST} of the structural transition (ST) can be defined by the equation $R(T_{ST})=1/3$, assuming that the relationship between R and T is known.

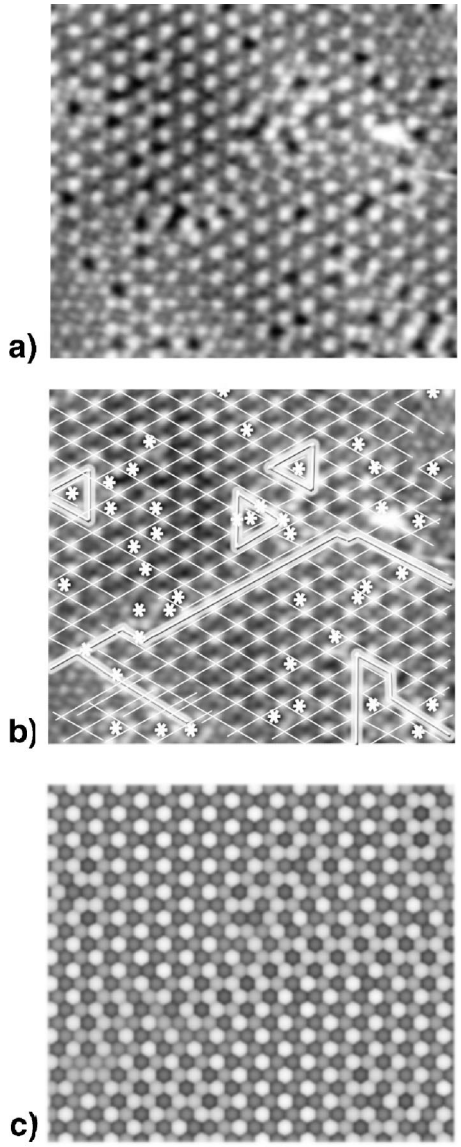

FIG. 6. Comparison of the LT STM and the CCM calculated images. (a) Experimental filled state constant current image (-1 V, 0.1 nA, 186×161 Å^2) obtained at $T=55$ K. (b) Labeling of (a) with (3×3) domains indicated by grids and the domain walls indicated by thick white lines, and Ge defects indicated by asterisks (*). (c) Image calculated by the CCM with Ge defects positioned as in the STM image (the CCF $R=0.34$, $a_3=0.1$).

(1) For $R>1/3$ the CCM reproduces domains and domain boundaries. Domains and domain walls in the STM image [Fig. 6(a)] and the calculated ones [Fig. 6(c)] coincide. To facilitate a comparison, domains (grids of thin white lines), domain walls (wide lines), and defects (asterisks) are indicated in Fig. 6(b). Knowing only the positions of defects we can reproduce the domain structure of these surfaces, i.e., defect positions determine domain size and shape. It is one of the indications of how strong the influence of defects is on these surfaces and a reminder that defects cannot be disregarded in the structure measurements.

(2) For $R<1/3$ the calculated STM images are the result of the superposition of exponentially decaying waves from

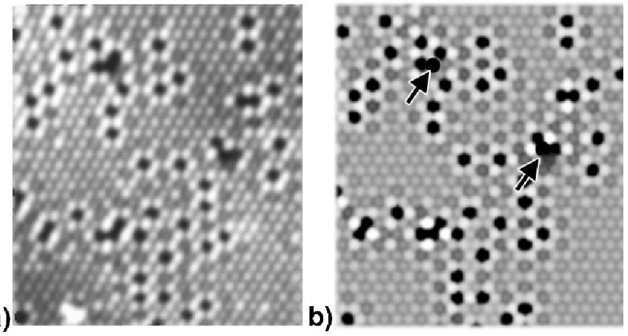

FIG. 7. Comparison of the RT STM and the CCM calculated images. (a) Filled state constant current STM image taken at RT (-1 V, 0.1 nA, 165×185 Å^2). (b) CCM calculated ($R=0.32$, $a_3=0.1$) with defects positioned as in (a). The arrows show two vacancies.

defects (Sec. II). Figure 7 displays a RT STM image (a) and the calculation (b). In this case the best match was obtained when $R=0.32$. Each Ge defect (black circles in Fig. 7) induces a local honeycomb (3×3) superstructure [as in Fig. 2(b)] and each vacancy [indicated by arrows in Fig. 7(b)] induces a hexagonal (3×3) superstructure that decays with the distance from a defect. We found that the best fit for the envelope function of this decay is an exponent

$$f(x)=A\times\exp(-x/l), \tag{8}$$

where x is a distance from a defect and l is a decay length that in a CCM calculation depends only on the value of the charge-compensation factor R. Calculating the best fit for each value of R we can obtain the dependence $l(R)$ measured in units of interatomic spacing. This result is shown in Fig. 8(a) for the case of Sn/Ge(111), in which the distance between NN atoms is 7 Å.

(3) The decay length increases with R and diverges at $R=1/3$. Such behavior describes very well the behavior of the Sn/Ge(111) system [Eq. (2)] that was determined experimentally by STM. This is another confirmation of the validity of the CCM. From the numerically calculated values of $l(R)$ [squares in Fig. 8(a)] it is reasonable to assume that $l(R)$ can be written as

$$l=A_R+\frac{B_R}{(R_c-R)^p}; \tag{9}$$

the best fit was obtained with an exponent $p=1/2$ [solid curve in Fig. 8(a)].

(4) We can infer $R(T)$ from the $l(R)$ and $l(T)$, determined theoretically and experimentally, respectively. The value of the decay length that we measured from RT STM images is $l(T=295\ \text{K})=11$ Å.[18] At the same time this decay length can be calculated for $R=0.32$ [$l(R=0.32)=11$ Å]. From Eqs. (2) and (9) we can obtain $R(T)$ using the definition that $R(T_{ST}=1/3)$:

$$l=A_R+\frac{B_R}{(R_c-R)^{1/2}}=A_T+\frac{B_T}{(T-T_{ST})}, \tag{10}$$

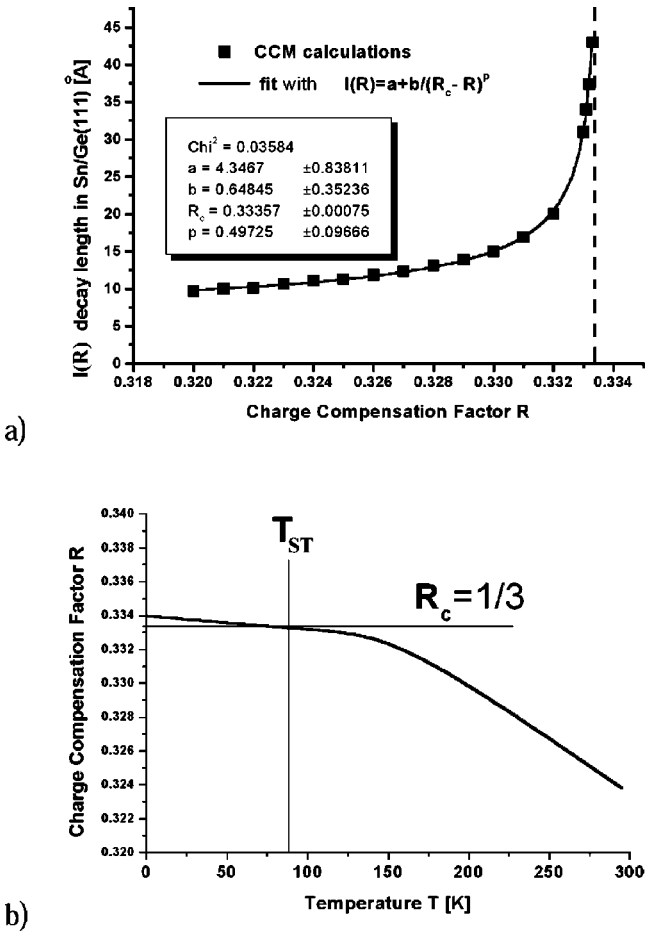

FIG. 8. Relation between the decay length, temperature, and CCF. (a) Plot of the relationship between the CCF R and the decay length $l(T)$. The fitted curve is a power-law function with the parameters shown in the box. (b) The dependence of the CCF R on temperature with an extrapolation below T_{ST}.

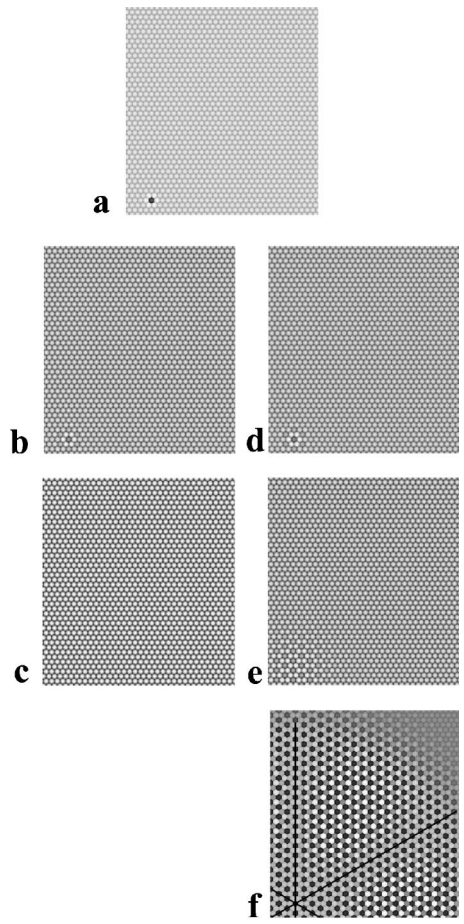

FIG. 9. Propagation of the solution with iterations with no defects. The images present charge maps for (a) initial conditions ($+1$ on a dark atom and $-1/6$ on its nearest neighbors), (b) after 10 iterations for $R=0.32$, (c) after 100 iterations for $R=0.32$, (d) after 10 iterations for $R=0.34$, (e) after 100 iterations for $R=0.34$, and (f) 500 iterations for $R=0.34$. a_3 was 0.1 for both $R=0.32$ and $R=0.34$ calculations.

where $T_{ST}=-\alpha/\beta$, $R_c=1/3$, $A_T=0$, and $B_T=1/\beta$. For temperatures lower than T_{ST} we can extrapolate $R(T)$ assuming that it is a smooth monotonous function of temperature. This is shown in Fig. 8(b).

(5) The dependence of the solution on initial conditions can be considered as an indication of an instability in the system. A very important characteristic of the response of the system for different charge-compensation factors can be observed in the evolution of CD maps with the increase of number of iterations with no defects present. Figure 9 illustrates such an evolution for two values of R: $R=0.32$ (left side) that is less than the critical value, and $R=0.35$ (right side) that is higher than the critical value. Before the iterations the charge on one atom was set to $+1$ and the NN atoms to $-1/6$. Here the charge $+1$ in the initial condition is considered a variable of the calculation. In the case of $R<1/3$ ($R=0.32$ in Fig. 9) the perturbation propagates for a very short distance and simultaneously its amplitude dies out and becomes zero in a few iterations. In the case of $R>1/3$ such a perturbation propagates indefinitely. In this particular case of $R=0.35$ at 100 iterations the honeycomb pattern forms for as far as ten (3×3) unit cells from the origin. The further iterating (500 iterations) leads to a solution with six domains with sharp domain walls. Inside each domain the solution is a configuration with one atom positive, one zero, and one negative in each (3×3) unit cell. As shown in the next section, such a charge arrangement in one (3×3) unit cell is the lowest-energy solution for this system. The symmetry of the initial perturbation and strong nonlinear response of the system leads to the formation of six domains for this value of R. Further increase of the number of iterations propagates this solution further until the boundaries of the computed area are encountered. It is important to note that in a case of the system with even just a few defects the solution is determined by their position and is independent of the initial conditions.

(6) A calculated structure has a (3×3) periodicity and it is a product of the geometry (triangular lattice) and the type of nearest-neighbor interaction. The (3×3) periodicity is not imposed on this system but is a result of a self-consistent solution of Eqs. (6) and (7) for a triangular lattice. It is similar to the problem of a frustrated antiferromagnetic on a triangular lattice.[23,36] The system prefers to have opposite

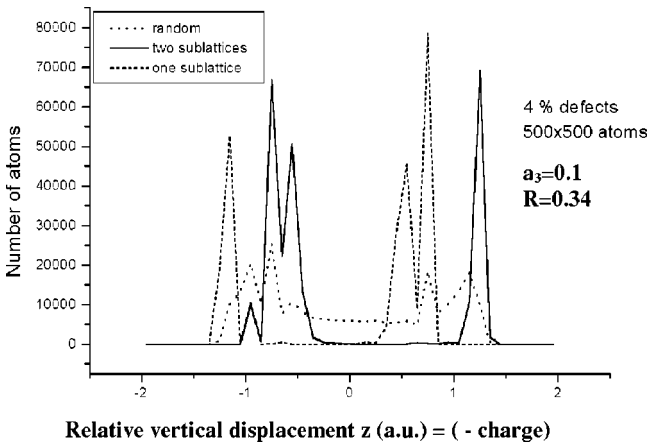

FIG. 10. Histograms of the distribution of out-of-plane displacement z for different states of the defect order calculated using the CCM with $R=0.34$, $a_3=0.1$, and a 4% density of defects. The dotted, solid, and dashed lines represent calculated distributions for randomly distributed defects, ordered on two (3×3) sublattices, and ordered on one (3×3) sublattice, correspondingly. The vertical displacement is assumed to be proportional to the charge calculated using the CCM. The sign of the z values are opposite to the signs of the charge and the z axis is directed outward from the surface.

charges on the nearest neighbors, which is not possible on a triangular lattice. Thus we can conclude that the symmetry of this solution is dictated by the geometry of the problem. Apparently, as shown here, a localized (nearest neighbors only) temperature-dependent response of the system coupled with the inherent geometry of the system (i.e., triangular lattice) dictates the (3×3) symmetry of the low-temperature phase.

(7) The (3×3) lattice structure is dictated by the specific defect alignment. It is commonly believed that the structure of the Sn/Ge(111) surface holds the key to understanding the origin of this phase transition.[6] Currently there is little agreement on the structure, determined by different groups. Most of the measurements show that at LT one atom is displaced outward from the surface (''up'') and two are displaced inward (''down'') in a (3×3) unit cell,[6,29] while one report shows that the structure is two ''up'' and one ''down.''[4] In the following we will show that the calculations suggest that the structure, determined by any area averaging technique, depends on the distribution of defects or, to be more exact, on their order. If we assume that the lattice distortion at an atomic site is proportional to the charge on this site we can calculate the height (vertical displacement) distribution of atoms for different arrangements of defects at LT using the CCM. Figure 10 shows the results of such calculations. The calculations are performed for a random defect distribution, for defects ordered on two sublattices out of three, and defects ordered on one sublattice out of three. For the random distribution of defects, atoms with almost any height/charge are present in equal quantity (dotted line). When the defects are ordered on two sublattices (as was observed by STM) there are three distinct peaks that correspond to 1/3 of atoms displaced up and 2/3 down (solid line). This supports the measurements of research groups that came to the conclusion that there is one up and two down Sn atoms in a unit cell. When defects are ordered on one sublattice the structure is two up and one down (dashed curve) supporting the recent x-ray-diffraction results.[4] In the absence of defects, according to the CCM we should expect one up, one down, and one in an undistorted position. Proper STM measurements have to be done to confirm this observation. Nevertheless this result indicates that the key to understanding this transition lies in the understanding of the influence of defects.

It is worthwhile to compare the CCM with the model that describes the surface as a linear superposition of defect-induced waves [Eq. (1)]. In this linear superposition model the defects are the only sources of waves, while in the CCM all the atoms induce waves in their vicinity proportional to their charges. In this respect all the lattice sites are treated equally. The distinction is only that the charges are allowed to vary on Sn atoms but are fixed on defect sites. In some sense the CCM is similar to the Hyugens principle in optics.

C. Equivalent formulation of the CCM in the framework of Ginzburg-Landau theory

We can approach the structural phase transition from the point of view of the Ginzburg-Landau (G-L) theory of phase transitions.[37] McMillan had applied G-L theory to the CDW phase transitions in transition-metal dichalcogenides.[38] His results have been used for calculations of STM images in layered compounds and comparison with experimental results.[39] In the following we will present similar considerations but restricted to a lattice.[40]

In order to describe the CCM in the framework of G-L theory let's consider a system that has the following free-energy dependence on order parameter $\{q_{i,j}\}$, the charge on each lattice site (i,j):

$$F=\sum_n \left(q_{i,j}^2+R(T)q_{i,j}\sum_{k,l=NN_{i,j}} q_{i,j}+a_4 q_{i,j}^4 \right). \qquad (11)$$

The first summation goes over all atoms in the lattice. The internal sum runs over the next-nearest neighbors of the (i,j)th site (six in case of a triangular lattice). We proceed by solving for the order parameters $q_{i,j}$, which minimize the free energy. This can be done by solving a system of equations:

$$\frac{\partial F}{\partial q_{i,j}}=2q_{i,j}+2R(T)\sum_{k,l=NN_{i,j}} q_{i,j}+4a_4 q_{i,j}^3. \qquad (12)$$

Essentially, the expressions (12) mean that the CCM described in Sec. III A is just a minimization procedure for a free-energy Eq. (11). For a pure system, the free-energy Eq. (11) for a triangular lattice has a minimum when the system has (3×3) periodicity and the charges of the atoms inside one (3×3) unit cell are c, 0, and $-c$, correspondingly with the value of c that can be obtained from substituting this form of solution into Eq. (12). As a result we obtain

$$F_{min} = \sum^{All(3\times3)} (2c^2 - 6Rc^2 + 2a_4c^4)$$

$$= 2 \sum^{All(3\times3)} [(1-3R)c^2 + a_4c^4]. \quad (13)$$

We make the usual assumption in Landau theory that the parameters in front of the powers of the order parameter are continuous functions of temperature and can be expanded in powers of $(T-T_0)$ near the onset temperature. Since the factor in front of c_2 must change sign near T_0, we assume that

$$a_2 = (1-3R) = a'(T-T_0). \quad (14)$$

Here a' is some constant. The expression (13) does not contain a cubic term. This means that Eq. (13) describes a second-order phase transition. Differentiation of free-energy per one (3×3) unit cell gives

$$\frac{\partial F_{(3\times3)}}{\partial c} = 4a_2c + 8a_4c^3 = 0 \quad (15)$$

that has two solutions of this minimization problem. Assuming that a_4 is small and positive, they are

$$c = 0 \quad \text{for} \quad a_2 > 0, \quad (16)$$

or

$$c^2 = -\frac{a_2}{2a_4} = -\frac{(1-3R)}{2a_4} \quad \text{for} \quad a_2 < 0. \quad (17)$$

D. Influence of defects on the nature of the structural $(\sqrt{3}\times\sqrt{3}) \Leftrightarrow (3\times3)$ transition

Computer simulations based on the CCM enable the investigation of the influence of defects on the structural phase transition. Figure 11(a) displays the dependence of the order parameter squared $q_{i,j}^2$ averaged over all atoms in a lattice, $Q(R)$, on the charge-compensation factor R across the phase transition in Sn/Ge(111) for different defect densities, ρ. The value of $Q(R)$ is calculated by

$$Q(R) = \frac{1}{N} \sum_{i,j}^{N} q_{i,j}^2 . \quad (18)$$

This calculation was performed for different densities of defects that are randomly distributed on a lattice. Figure 11(b) shows the same curves in terms of temperature. The transformation was made using Eq. (10). The following conclusions are deduced from Fig. 11:

(1) $(\rho = 0\%)$ The structural phase transition in a system with zero defects exists and is a second-order transition. The dashed black line is the solution for zero defects (density of defects $\rho = 0\%$), which can also be calculated from Eqs. (16) and (17). It is equal to zero for the values of R up to $R_c = 1/3$ and then increases linearly. This indicates the existence of a structural phase transition at $R_c = 1/3$ and at the corresponding temperature.

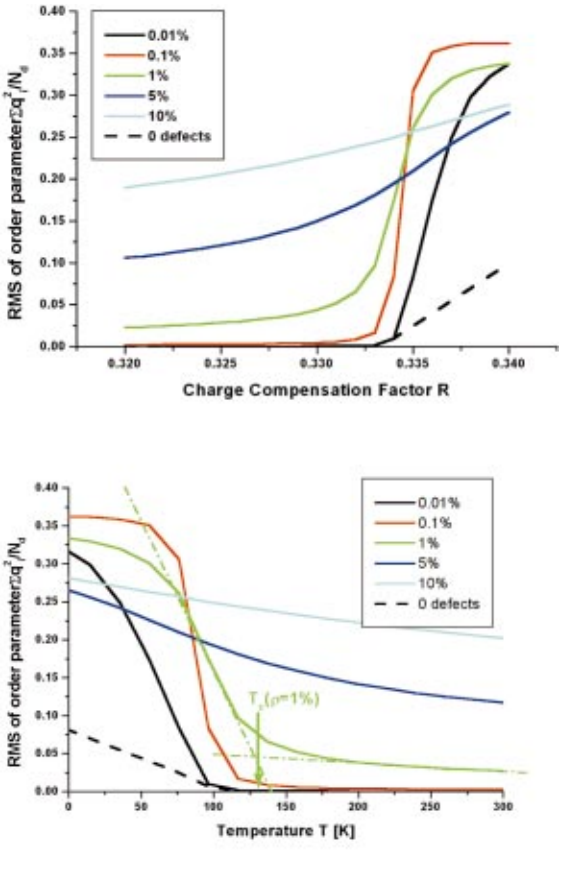

FIG. 11. (Color) The order parameter squared and averaged over all atoms in a lattice versus (a) the CCF R and (b) temperature T for different densities of defects calculated using the CCM with $a_3 = 0.1$. The defects are randomly distributed on all the three (3×3) sublattices shown in Fig. 2.

(2) $(\rho < 5\%)$ There is no structural phase transition but we can distinguish two pseudophases. The calculations show that any number of defects destroys the structural phase transition since the order parameter in not zero at any temperature. Since the two different phases are still distinguishable by the change in the slope of the free energy and the order-parameter dependence on temperature, one can talk about a crossover for the system with fixed defects. The critical value of $R_c(\rho)$ and the corresponding crossover temperature $T_c(\rho)$ can be determined as the intersection of the linear fit to the two portions of the $Q(R)$ curve, for $R > 1/3$ and $R < 1/3$. A small number of defects [0.001% (blue line)] increases the slope of the linear dependence for $R > 1/3$ compared to zero defects. The $T_c(\rho)$ stays the same as T_{ST} in this case. Further increase in the defect density (0.1%–5%) increases the slope and shifts the crossover region to higher temperature. From these results we can conclude that for defect density above 1% the crossover temperature is above 200 K, while for zero defect density, it is around 70 K. It was originally reported that the transition temperature measured by LEED was 210 K. The STM measurements based on the temperature dependence of the decay length showed that the structural transition in the absence of defects would be at 70 K. This large difference in T_C is due to the influence of defects.

(3) ($\rho > 5\%$) The high- and low-temperature phases are indistinguishable. When the density of defects is very high (e.g., 10%) two phases become almost indistinguishable. It is impossible to determine the crossover temperature from the curves for 5% and 10% in Fig. 11(b). In this case the range of the defect-induced DW's is comparable with the average distance between defects.

(4) Calculations of $Q(R)$ for defects distributed randomly on two of the three sublattices give qualitatively similar results as presented in Fig. 11. Even though in the system with fixed defects there is no structural phase transition, there is still a phase transition in Sn/Ge(111), since the defects are mobile and interacting. The accompanying disorder-order phase transition in the defect distribution creates a long-range order in this system by coupling phases of waves created by defects via alignment of defect positions in a lattice. Calculations with the charge-compensation model and the model that accounts for defect ordering should give a more precise picture for this complex transition. Such a calculation was beyond our current computational resources. Also for such a complex transition a different order parameter can be chosen, e.g., phase of the waves. The nucleation and possible hysteresis associated with an activation barrier for the defect motions lets us conclude that this phase transition is the first-order transition.

IV. CONCLUSIONS

Two phenomenological models presented in this paper describe the role of defects in phase transitions that constitute a complex symmetry lowering phase transition observed experimentally in such systems as Sn/Ge(111). The defect-ordering transition model is based on the observations that defects induce DW's, the range of these waves increases with decreasing temperature, and defects interact with these waves resulting in defect alignment with the DW's. The charge-compensation model describes the structural transition in the presence of defects, based on the assumption that the charge on an atomic site is a function of the total charge on its nearest neighbors. Treating defects as atoms with a fixed nonzero charge, the CCM allows calculation of the defect-induced waves, the domains, the domain walls, and the lattice structure of (3×3) unit cells just based on the spatial defect distribution. These results show how dramatic an effect the presence of deflects can have on a 2D phase transition. In fact, without the defect-ordering transition there would be no phase transition since the order parameter never becomes zero. This situation is similar to ferromagnetism where one can speak about long-range order only inside one domain. Due to the alignment of defects inside each domain and the formation of the domains the long-range order is created inside each domain and a phase transition in Sn/Ge(111) exists.

ACKNOWLEDGMENTS

We would like to thank A. L. Chernyshev and M-Y. Chou for fruitful discussions. A.V.M. would like to thank S. King for help in usage of the PC cluster in the Solid State Division of Oak Ridge National Laboratory. The work of E.W.P. and A.V.M. was supported by the National Science Foundation (NSF) Grant No. DMR 0105232. A portion of this work was conducted at Oak Ridge National Laboratory, managed by UT-Battelle, LLC, for the U.S. Deptartment of Energy under Contract No. DE-AC05-00OR22725, NSF, and UT-Battelle.

*Present address: Telephia, Inc., 1 Beach Street, San Francisco, CA 94133.

†Present address: Infineon Technologies, München, Germany, D-81609.

[1] B. I. Halperin and C. M. Varma, Phys. Rev. B **14**, 4030 (1976).

[2] H. Mutka, in *Advances in the Crystallographic and Microstructural Analysis of Charge Density Wave Modulated Crystals*, edited by F. W. Boswell and J. C. Bennet (Kluwer, Dordrecht, 1999).

[3] I. Baldea and M. Badescu, Phys. Rev. B **48**, 8619 (1993).

[4] J. Avila, A. Mascaraque, G. Le Lay, E. G. Michel, M. Gothelid, H. Ascolani, J. Alvarez, S. Ferrer, and M. C. Asensio (unpublished).

[5] J. Avila, A. Mascaraque, E. G. Michel, M. C. Asensio, G. LeLay, J. Ortega, R. Perez, and F. Flores, Phys. Rev. Lett. **82**, 442 (1999).

[6] O. Bunk, J. H. Zeysing, G. Falkenberg, R. L. J. H. Zeysing, G. Falkenberg, R. L. Johnson, M. Nielsen, M. M. Nielsen, and R. Feidenhansl, Phys. Rev. Lett. **83**, 2226 (1999).

[7] J. M. Carpinelli, H. H. Weitering, M. Barkowiak, R. Stumpf, and E. W. Plummer, Phys. Rev. Lett. **79**, 2859 (1997).

[8] J. M. Carpinelli, H. H. Weitering, E. W. Plummer, and R. Stumpf, Nature (London) **381**, 398 (1996).

[9] F. Flores, J. Ortega, and R. Perez, Surf. Rev. Lett. **6**, 411 (1999).

[10] A. Goldoni and S. Modesti, Phys. Rev. Lett. **79**, 3266 (1997).

[11] T. E. Kidd, T. Miller, and T. C. Chiang, Phys. Rev. Lett. **83**, 2789 (1999).

[12] T. E. Kidd, T. Miller, M. Y. Chou, and T. C. Chiang, Phys. Rev. Lett. **85**, 3684 (2000).

[13] G. Le Lay, V. Y. Aristov, O. Bostrom, J. M. Layet, M. C. Asensio, J. Avila, Y. Huttel, and A. Cricenti, Appl. Surf. Sci. **123**, 440 (1998).

[14] A. Mascaraque, J. Alvarez, J. Avila, M. C. Asensio, S. Ferrer, and E. G. Michel, Surf. Sci. **454**, 191 (2000).

[15] A. Mascaraque, J. Avila, J. Alvarez, M. C. Asensio, S. Ferrer, and E. G. Michel, Phys. Rev. Lett. **82**, 2524 (1999).

[16] A. Mascaraque, J. Avila, M. C. Asensio, and E. G. Michel, Surf. Sci. **404**, 742 (1998).

[17] A. Mascaraque, J. Avila, M. C. Asensio, and E. G. Michel, Surf. Sci. **435**, 337 (1999).

[18] A. V. Melechko, J. Braun, H. H. Weitering, and E. W. Plummer, Phys. Rev. Lett. **83**, 999 (1999).

[19] A. V. Melechko, J. Braun, H. H. Weitering, and E. W. Plummer, Phys. Rev. B **61**, 2235 (2000).

[20] J. Ortega, R. Perez, and F. Flores, J. Phys.: Condens. Matter **12**, L21 (2000).

[21] L. Ottaviano, M. Crivellari, L. Lozzi, M. Passcantando, P. Picozzi, and S. Santucci, J. Vac. Sci. Technol. A **18**, 1946 (1999).

[22] L. Ottaviano, M. Crivellari, L. Lozzi, and S. Santucci, Surf. Sci. **445**, L41 (2000).
[23] G. Santoro, S. Scandolo, and E. Tosatti, Phys. Rev. B **59**, 1891 (1999).
[24] S. Scandolo, F. Ancilotto, G. L. Chiarotti, G. Santoro, S. Serra, and E. Tosatti, Surf. Sci. **404**, 808 (1998).
[25] R. I. G. Uhrberg and T. Balasubramanian, Phys. Rev. Lett. **81**, 2108 (1998).
[26] R. I. G. Uhrberg, H. M. Zhang, and T. Balasubramanian, Phys. Rev. Lett. **85**, 1036 (2000).
[27] R. I. G. Uhrberg, H. M. Zhang, T. Balasubramanian, S. T. Jemander, N. Lin, and G. V. Hansson, Phys. Rev. B **62**, 8082 (2000).
[28] H. H. Weitering, J. M. Carpinelli, A. P. Melechko, J. D. Zhang, M. Bartkowiak, and E. W. Plummer, Science **285**, 2107 (1999).
[29] J. D. Zhang, Ismail, P. J. Rous, A. P. Baddorf, and E. W. Plummer, Phys. Rev. B **60**, 2860 (1999).
[30] M. Gothelid, M. Hammar, C. Tornevik, U. O. Karlsson, N. G. Nilsson, and S. A. Flodstrom, Surf. Sci. **271**, L357 (1992).
[31] J. M. Carpinelli, H. H. Weitering, and E. W. Plummer, Surf. Sci. **401**, L457 (1998).
[32] T. Yamanaka and S. Ino, Phys. Rev. B **61**, R5074 (2000).
[33] L. Floreano, L. Petaccia, M. Benes, D. Cvetko, A. Goldoni, R. Gotter, L. Grill, A. Morgante, A. Verdini, and S. Modesti, Surf. Rev. Lett. **6**, 1091 (1999).
[34] In the following we will describe only filled state STM images since empty state STM images are complimentary and can be obtained by inversion of the result.
[35] A solution that is independent of the boundary conditions for a special case of zero defects and large values of R (discussed later) is possible to achieve only if iterations are stopped before the solution in the middle of the area is affected by the boundaries. Thus the much larger area is used for such calculations and only the central part is taken into consideration.
[36] J. P. Rodriguez and E. Artacho, Phys. Rev. B **59**, R705 (1999).
[37] V. L. Ginzburg and L. D. Landau, Zh. Éksp. Teor. Fiz. **20**, 1064 (1950).
[38] W. L. McMillan, Phys. Rev. B **12**, 1187 (1975).
[39] G. Vanbakel and J. T. M. Dehosson, Phys. Rev. B **46**, 2001 (1992).
[40] M. LeBellac, *Quantum and Statistical Field Theory* (Clarendon Press, Oxford, 1991), Chap. 2.